Behavioral/Cognitive

An fMRI-Based Brain Marker of Individual Differences in Delay Discounting

Leonie Koban,[1,2,3] Sangil Lee,[4] Daniela S. Schelski,[5,6] Marie-Christine Simon,[7] Caryn Lerman,[8] Bernd Weber,[5,6] Joseph W. Kable,[4] and Hilke Plassmann[1,2]

[1]Marketing Area, INSEAD, F-77300 Fontainebleau, France, [2]Control-Interoception-Attention Team, Paris Brain Institute (ICM), INSERM U1127, CNRS UMR7225, Sorbonne University, 75013 Paris, France, [3]CNRS, INSERM, Centre de Recherche en Neurosciences de Lyon CRNL U1028 UMR5292, Université Claude Bernard Lyon 1, 69500 Bron, France, [4]Department of Psychology, University of Pennsylvania, Philadelphia, Pennsylvania 19104-6018, [5]Center for Economics and Neuroscience, University of Bonn, 53113 Bonn, Germany, [6]Institute of Experimental Epileptology and Cognition Research, University of Bonn Medical Center, 53113 Bonn, Germany, [7]Institute for Nutrition and Food Science, Nutrition and Microbiota, University of Bonn, 53113 Bonn, Germany, and [8]Norris Comprehensive Cancer Center, University of Southern California, Los Angeles, California 90033

Individual differences in delay discounting—how much we discount future compared to immediate rewards—are associated with general life outcomes, psychopathology, and obesity. Here, we use machine learning on fMRI activity during an intertemporal choice task to develop a functional brain marker of these individual differences in human adults. Training and cross-validating the marker in one dataset (Study 1, $N = 110$ male adults) resulted in a significant prediction–outcome correlation ($r = 0.49$), generalized to predict individual differences in a completely independent dataset (Study 2: $N = 145$ male and female adults, $r = 0.45$), and predicted discounting several weeks later. Out-of-sample responses of the functional brain marker, but not discounting behavior itself, differed significantly between overweight and lean individuals in both studies, and predicted fasting-state blood levels of insulin, c-peptide, and leptin in Study 1. Significant predictive weights of the marker were found in cingulate, insula, and frontoparietal areas, among others, suggesting an interplay among regions associated with valuation, conflict processing, and cognitive control. This new functional brain marker is a step toward a generalizable brain model of individual differences in delay discounting. Future studies can evaluate it as a potential transdiagnostic marker of altered decision-making in different clinical and developmental populations.

Key words: **brain model; decision-making; delay discounting; fMRI; neuroeconomics; prediction**

Significance Statement

People differ substantially in how much they prefer smaller sooner rewards or larger later rewards such as spending money now versus saving it for retirement. These individual differences are generally stable over time and have been related to differences in mental and bodily health. What is their neurobiological basis? We applied machine learning to brain-imaging data to identify a novel brain activity pattern that accurately predicts how much people prefer sooner versus later rewards, and which can be used as a new brain-based measure of intertemporal decision-making in future studies. The resulting functional brain marker also predicts overweight and metabolism-related blood markers, providing new insight into the possible links between metabolism and the cognitive and brain processes involved in intertemporal decision-making.

Received July 8, 2022; revised Dec. 2, 2022; accepted Dec. 7, 2022.

Author contributions: L.K., M.-C.S., C.L., B.W., J.W.K., and H.P. designed research; D.S.S. performed research; L.K. and S.L. analyzed data; L.K. wrote the paper.

Funding for the research was received from the French National Research Agency [ANR; Tremplin-ERC Grant "Brain Gut Decision" to H.P.], Campus France (Marie- Skłodowska-Curie co-fund Fellowship PRESTIGE-2018-2-0023 to L.K.), French federal funding (program "Investissements d'avenir" ANR-10-IAIHU-06), the Federal Ministry of Education and Research Germany (Diet-Body-Brain Grants 01EA1809B to B.W. and 01EA1707 to M.-C.S), the National Cancer Institute [Grants R35-CA-197461 (to C.L.) and R01-CA-170297 (to J.W.K. and C.L.)], and the AE Foundation (to J.W.K.). The funders had no role in study design, data collection and analysis, decision to publish, or preparation of the manuscript. We thank P. Trautner for help with the programming of the task (Study 1); A. Simonetti, M. Boerth, J. Tholen, A.-A. Ortner, A. Koehlmoos, S. Winkler, L. Bernardo, A. M. Burke, M. K. Caulfield, N. Cooper, G. Donnay, M. Falcone, J. Jorgensen, R. Kazinka, J. Luery, M. McConnell, R. Miglin, D. Mukherjee, T. Parthasarathi, S. Price, M. Schlussel, R. Sharp, H. J. Sohn, D. Spence, and K. Terilli for help with data acquisition; and T. D. Wager for the CANLab toolbox and helpful discussion.

The authors declare no competing financial interests.

Correspondence should be addressed to Leonie Koban at leonie.koban@cnrs.fr.

https://doi.org/10.1523/JNEUROSCI.1343-22.2022

Copyright © 2023 the authors

Introduction

Many decisions in life have consequences at different points in time. For example, most people need to decide whether to put part of their paycheck toward a retirement fund or spend it on something fun, like a short vacation. These trade-offs between options that are immediately rewarding and those that will be more rewarding in the long run are hard, and people differ substantially in delay discounting—the degree to which they discount future compared with immediate rewards (Kirby and Herrnstein, 1995). Greater delay discounting (i.e., greater impatience or higher preference for sooner rewards) is associated with obesity, addiction, and many psychiatric conditions (Bickel et al., 1999; MacKillop et al., 2011; Mole et al., 2015; Amlung et al., 2016). It has therefore been proposed as a potential transdiagnostic marker of psychopathology (Amlung et al., 2019; Lempert et al., 2019) and as a risk factor for short-sighted behaviors such as unhealthy diet, smoking, and excessive alcohol and drug use (Audrain-McGovern et al., 2009; Fernie et al., 2013). The goal of the present study is to identify and validate an fMRI-based brain marker of individual differences in delay discounting.

Previous findings regarding the structural and functional brain bases of individual differences in delay discounting offer a mixed picture. Several studies suggest a role for areas involved in reward processing and valuation (Bartra et al., 2013; Cooper et al., 2013), and for areas central to cognitive control (Hare et al., 2014). Brain areas associated with memory and prospection have also been found to contribute to individual differences in delay discounting (Benoit et al., 2011; Peters and Büchel, 2011; Lebreton et al., 2013). Studies using structural and functional connectivity measures suggested a role for frontal–striatal and striatal–subcortical connections (van den Bos et al., 2014). The structure of midbrain dopaminergic nuclei and the ventral striatum has been associated with self-reported trait impulsivity (MacNiven et al., 2020).

Individual differences in delay discounting may also emerge from the combined activity across multiple brain regions or functional networks. However, only a few studies (Berman et al., 2013; Li et al., 2013; Pehlivanova et al., 2018) have investigated the distributed patterns associated with individual differences in delay discounting. Further, most previous studies used relatively small sample sizes to explore these individual differences, increasing the risk of both false-positive and false-negative results (Poldrack et al., 2017). Given the use of standard correlation or regression analyses that are typically not cross-validated on independent data samples, previous results are difficult to compare with each other and do not provide any formal model that could predict delay discounting in completely independent studies.

Here, we address these limitations by using a machine learning-based "brain model" approach (Woo et al., 2017; Kragel et al., 2018). Brain models are trained to predict a mental process or individual variable (here, delay discounting) and can be applied to independent data (Kragel et al., 2018; Scheinost et al., 2019). As such, brain models go beyond reporting peak coordinates by identifying specific large-scale patterns of brain activity that can be replicated, validated, or falsified in a quantifiable way. This approach has been successfully applied to brain-based prediction of pain (Wager et al., 2013), working memory (Rosenberg et al., 2020), and affective states (Yu et al., 2020), among others. The importance of independent validation and model generalizability has also been recognized for brain-based prediction of trait-like individual differences (Gabrieli et al., 2015; Rosenberg et al., 2018; Rosenberg and Finn, 2022).

Here, we build on this approach to predict individual differences in delay discounting. If there is a consistent activity pattern associated with individual differences in delay discounting during intertemporal choices, then this pattern should be able to predict delay discounting in new data (hold-out subjects) and even completely independent datasets. Comparing the resulting pattern to meta-analysis-based masks allows us to assess the contribution of brain areas associated with valuation, cognitive control, and prospection.

Materials and Methods

Overview

We used an established machine-learning algorithm, LASSO-PCR (least absolute shrinkage and selection operator-principal component regression; Tibshirani, 1996; Wager et al., 2011), and fMRI data from two independent studies, from different scanners, laboratories, and countries. Study 1 ($N = 110$) was used for training and cross-validation of a predictive model of individual differences in delay discounting. Study 2 [existing dataset from a previously published study (Kable et al., 2017); $N = 145$] was used as an independent test dataset to assess the validity and replicability of the predictive model.

Participants

For Study 1, participants were recruited in the context of a 7 week dietary intervention study at the University of Bonn (Bonn, Germany; https://osf.io/rj8sw/?view_only=af9cba7f84064e61b29757f768a8d3bf). Because of the nature of this longitudinal intervention study, we recruited only male participants who further fulfilled the following inclusion criteria: age between 20 and 60 years, right-handed, nonsmoker, no excessive drug or alcohol use in the past year, no psychiatric or neurologic disease, body mass index (BMI) between 20 and 34, no other chronic illness or medication, following a typical Western diet without dietary restrictions, and no MRI exclusion criteria (e.g., large tattoos, nonremovable piercings, metal in the body, claustrophobia). One hundred sixteen male participants performed the intertemporal choice task in Study 1. Here, we focus on behavioral and fMRI data collected during a baseline session before the group assignment and dietary intervention (to be reported elsewhere) and use post intervention behavioral data only for demonstrating the temporal stability of interindividual differences in delay discounting. The data from six participants had to be excluded for analysis for the following reasons: technical problems with the scanner (one participant), with the synchronization between stimulation software and scanner (three participant), and with the response box (one participant); strong motion artifacts (>5 mm) and participant quitting the task midscan (one participant). Therefore, 110 participants (mean age, 31.7 years; 52 lean, 48 overweight, and 10 obese participants; BMI range, 20.6–33.7) were included in the final analysis of Study 1. There were no significant differences between lean and overweight-to-obese participants in age, education, or total brain volume (Table 1). Data from 109 participants were available for the 7 week follow-up measurements (i.e., one participant did not return for the second session).

Study 2 was conducted in the context of a large cognitive training study at the University of Pennsylvania (Philadelphia, PA; Kable et al., 2017). The goal was to examine whether commercial cognitive training software leads to significant changes in decision-making behaviors, including delay discounting. Participants completed two sessions of scans 10 weeks apart. As with Study 1, we focus on the baseline (pre intervention) behavioral and fMRI data, and report postintervention behavioral data only to assess the temporal (10 week) stability of interindividual differences in delay discounting. Of the 160 nonpilot participants who completed session 1, we excluded those with missing runs ($N = 6$), frequent or significant head movement (any run with >5% of mean image displacements, >0.5 mm; $N = 3$), more than three missing trials per run for two or more runs ($N = 2$), or lack of participant blinding ($N = 1$; one subject expressed awareness of their experimental condition; i.e., cognitive training vs control). Of the remaining 148, we excluded 3 more participants whose choice was entirely one sided (i.e., choosing only immediate reward or delayed reward), resulting in a final sample of $N = 145$ participants for Study 2 (88 male, 57 female; mean age, 24.4 years; 81 lean, 39 overweight,

Table 1. Person-level characteristics of lean (BMI ≤ 25) and overweight-to-obese (BMI > 25) participants in Study 1 and Study 2

	BMI ≤ 25 Mean (SD)	BMI > 25 Mean (SD)	Two-sample *t* test		
			$t_{(df)}$	*p*-value	CI
Study 1	(*N* = 52)	(*N* = 58)			
BMI	23.0 (1.3)	27.8 (2.2)	−13.8 (108)	<0.001*	−5.51, −4.13
Log(k)	−5.71 (1.83)	−5.70 (2.04)	−0.04 (108)	0.96	−0.75, 0.72
k-marker	−5.87 (0.76)	−5.46 (0.74)	−2.85 (108)	0.005*	−0.69, −0.12
Age (years)	30.8 (10.4)	32.4 (9.8)	−0.85 (108)	0.40	−5.43, 2.17
Education (ordinal scale)	5.09 (2.71)	5.05 (2.89)	0.08 (108)	0.93	−1.02, 1.11
Total brain volume (l)	1.17 (0.09)	1.18 (0.09)	−0.62 (108)	0.53	−0.04, 0.02
Study 2	(*N* = 81)	(*N* = 64)			
BMI	22.2 (1.8)	29.4 (3.9)	−14.9 (143)	<0.001*	−8.18, −6.27
Log(k)	−4.09 (1.00)	−4.08 (0.83)	−0.08 (143)	0.94	−0.32, 0.30
k-marker	−5.86 (0.90)	−5.57 (0.74)	−2.1 (143)	0.037*	−0.57, −0.02
Age	24.2 (4.5)	24.6 (4.5)	−0.57 (143)	0.57	−1.93, 1.07
Education	3.31 (0.93)	3.39 (0.81)	−0.56 (143)	0.58	−0.37, 0.21
Total brain volume (l)	1.26 (0.12)	1.26 (0.12)	−0.11 (143)	0.91	−0.04, 0.04
Sex			χ^2 test	*p*-value	
Male (*N*)	46	42	1.17 (1)	0.28	
Female (*N*)	35	22			

Significant group differences are indicated by asterisks. Except for body mass index (by definition) and k-marker responses, none of the variables differed significantly between the two groups.

and 25 obese participants; BMI range, 16.5–40.9). There were no significant differences between lean and overweight-to-obese participants in sex, age, education, or total brain volume (Table 1). Because of dropout, data from 102 participants were available for the 10 week postintervention measurement of log(k).

The study protocols were approved by the institutional review boards of the Bonn University Medical School (Study 1) and the University of Pennsylvania (Study 2). All participants provided written informed consent, and were paid for their time and participation in the study. The research reported here complies with all relevant ethical regulations.

Stimuli and task

In Study 1, participants performed 108 choices (trials) between varying amounts of smaller sooner (SS) and larger later (LL) options, presented on the left or right of the screen (position randomized; Fig. 1*a*). Participants were instructed that one of their choices might be paid out at the end of the experiment. Thus, participants' choices were nonhypothetical and incentive compatible. During each trial, the two options were presented for 4 s, during which participants could make their choice (left or right) by pressing the corresponding response key with their left or right index finger, respectively. Once the choice had been made, a yellow frame highlighted the chosen option and remained on the screen for the remainder of the 4 s. Intertrial intervals were jittered using an approximately geometric distribution (2–11 s).

SS options varied among €5, €10, and €20, and always had zero delay ("today"). LL options varied between €5 and €96.80 and had delays between 2 d and 8 months (~240 d; Extended Data Fig. 1-1, choice combinations). Amounts and delays were chosen to allow fine-grained estimation of individual k values between 0 and 0.256. Trials were presented in randomized order.

The intertemporal choice task in Study 2 consisted of 120 trials, again with the same choice sets for all participants (Extended Data Fig. 1-2). In contrast to Study 1, the SS amount was fixed at $20 US. Thus, participants were presented with the LL option (with amount ranging from $22 to $85 US and delays from 19 to 180 d) and were instructed to press one of two keys to either accept and receive this LL offer or to reject the LL offer and receive the SS offer ($20 today) instead. Participants were informed that one trial would be randomly chosen at the end of the experiment and their choices implemented (i.e., the chosen amount would be paid via wire transfer at the indicated time delay), resulting in incentive-compatible and mutually independent choices in each trial (as in Study 1).

Blood measures and body fat measures

In Study 1, blood samples in a fasted state were collected from participants' nondominant arm before they received a standardized breakfast. Homeostatic model assessment for insulin resistance (HOMA-IR; a marker of insulin resistance) was calculated as the product of fasting insulin and glucose levels, divided by 405 (Lozano et al., 2012). Body weight and proportion of body fat were measured using a bioimpedance scale (Tanita Europe). For technical reasons, this body fat measure was available for only 103 participants.

Experimental design and statistical analyses

Behavioral measures. For each participant, we calculated the proportion of SS choices (with respect to the total number of nonmisses) and the model-based discounting parameter k. Individual k values were log transformed in both studies to obtain less skewed distributions of discounting parameters. This log(k) parameter describes the steepness of discounting as modeled by the hyperbolic discounting function (Kirby and Herrnstein, 1995). Higher log(k) parameters reflect steeper discounting and thus greater impatience; smaller (more negative) values reflect less steep discounting and thus more patient decision-making.

In Study 1 we computed k by calculating the proportion of SS choices for all target k values (i.e., the k value for which SS and LL options of any given choice trial should theoretically be chosen at 50% each). We then used linear interpolation to identify the individual indifference point at which the proportions of SS and LL choices were equal (50% each).

In Study 2, we fit a logit utility model on choice data via maximum likelihood estimation. The logit of the probability of choosing the delayed reward was modeled as follows:

$$\text{logit}\Big(p(Y_t = \text{delayed})\Big) = \sigma\left(\frac{\text{LL}_t}{1 + \text{kD}_t} - 20\right),$$

where LL_t is the LL amount in trial t and D_t is the delay in trial t. σ was included as a scaling parameter that controls the relationship between the utility difference scale and choice.

MRI data acquisition. Functional and structural brain imaging data for Study 1 were acquired using a Trio 3 T scanner (Siemens) at the Life & Brain Institute, Bonn University Hospital. Functional images used a T2*-weighted echoplanar imaging (EPI)-generalized autocalibrating partial parallel acquisition sequence (TR = 2.5 s; TE = 30 ms; flip angle = 90°; FOV = 192 mm; acceleration factor $R = 2$; average, 400 volumes) and covered the whole brain in 37 slices (voxel size, $2 \times 2 \times 3$ mm; 10% interslice distance). Structural images were acquired using a T1-weighted MPRAGE sequence (1 mm isomorphic voxels).

For Study 2, the functional and structural imaging data were acquired with a 3 T Trio scanner (Siemens) with a 32-channel head coil. High-resolution T1-weighted anatomic images were acquired using an MPRAGE sequence (T1 = 1100 ms; 160 axial slices; $0.9375 \times 0.9375 \times 1.000$ mm; 192×256 matrix). T2*-weighted functional images were acquired using an EPI sequence with 3 mm isotropic voxels [64×64 matrix; TR = 3 s; TE = 25 ms; 53 axial slices (no interslice gaps); 104 volumes]. B0 field map images were collected for distortion correction (TR = 1270 ms; TE = 5 and 7.46 ms).

Preprocessing and basic statistical analyses of fMRI data. Preprocessing for Study 1 was performed in SPM12 and used a standard pipeline of motion correction, slice time correction, spatial normalization to MNI space, and spatial smoothing of images using an 8 mm FWHM Gaussian kernel. Preprocessing for Study 2 was performed in FSL according to the original preprocessing pipeline (Kable et al., 2017). This involved the standard pipeline of motion correction, b0 map unwarping, interleaved slice time correction, spatial smoothing with a 9 mm FWHM Gaussian kernel, and high-pass filtering (cutoff = 104 s).

For Study 1, we used SPM12 to fit a general linear model for each participant's imaging data, with choice screen onset modeled as a stick function (0 s duration) as the main regressor and mean-centered parametric

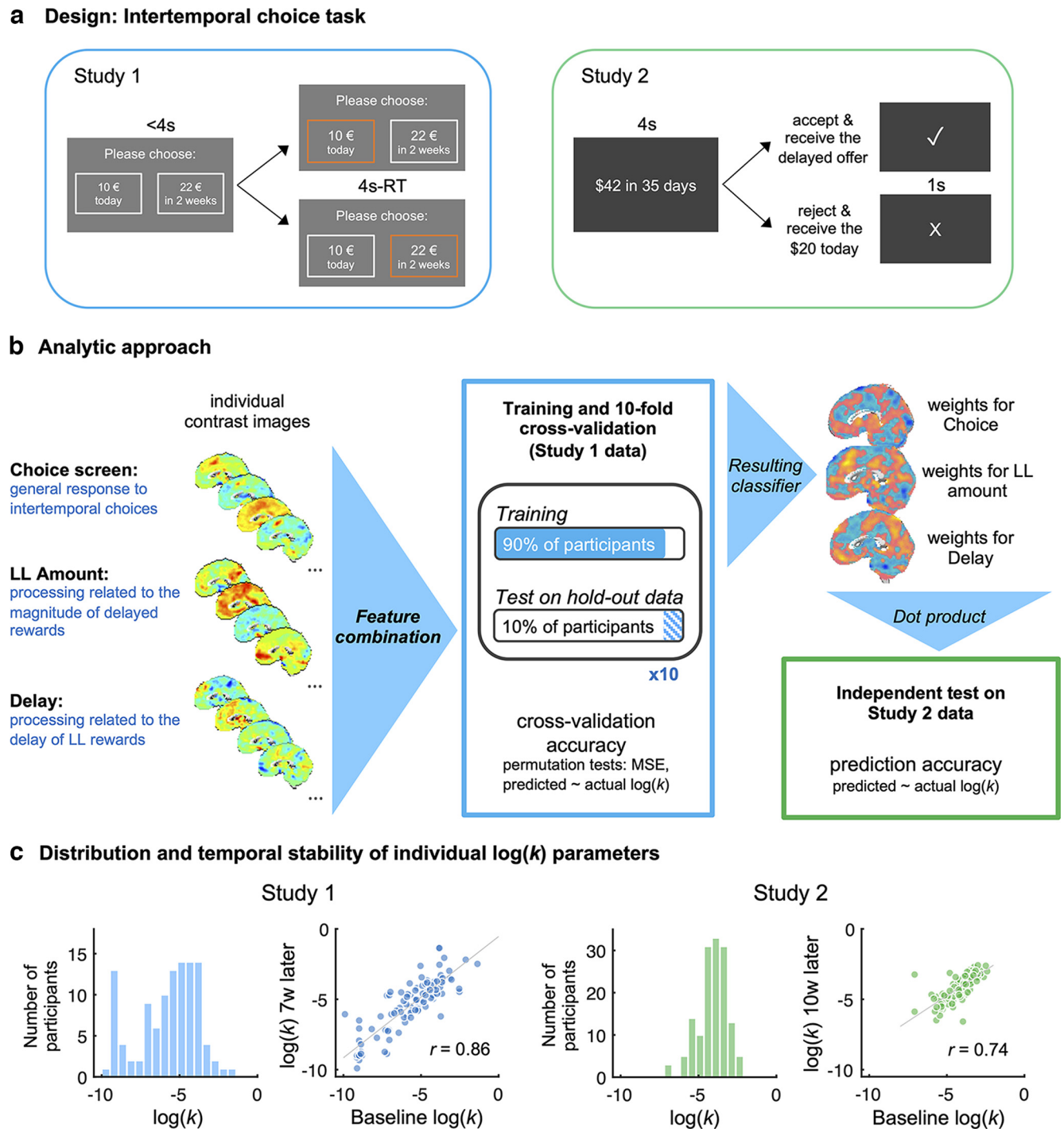

Figure 1. Experimental design, analytical approach, and discounting behavior. ***a***, Visual presentation of the intertemporal choice tasks and their timing in Study 1 and Study 2. All combinations of amounts and delays can be found in tables in Extended Data Figure 1-1 (for Study 1) and Extended Data Figure 1-2 (for Study 2). ***b***, Analytic approach. Contrast images for brain activity in response to the onset of the Choice screen and its parametric modulation by LL Amount and Delay were computed for each participant and concatenated. Data from Study 1 was used for training and 10-fold cross-validation. In each fold, the classifier was trained on 90% of the data using LASSO-PCR and tested on the remaining 10% holdout data to evaluate its predictive accuracy. The predictive classifier obtained from Study 1 was then tested on Study 2 data, acquired on a different scanner, in a different laboratory and country, assessing its validity in a completely independent dataset. ***c***, Distribution and temporal stability of individual log-transformed k-parameters by study. Scatterplots show high correlations between individual differences in discounting at baseline and several weeks later (Study 1: $N = 110$, $r = 0.86$, $p = 0.001$, 95% CI = 0.80, 0.90; Study 2: $N = 145$, $r = 0.74$, $p = 0.001$, 95% CI = 0.63, 0.82).

modulators for delay, relative LL amount (LL amount divided by SS amount), SS amount, and reaction time. Six nuisance regressors were added to control for movement artifacts. For Study 2, FSL was used to fit an otherwise similar statistical model with a choice screen onset as the main regressor, and mean-centered parametric modulators for delay, LL amount, and reaction time. As in Study 1, six movement regressors were added to control for head movement.

Individual contrast images were calculated for the following three regressors of interest that were available for both studies: (1) choice screen onset versus implicit baseline (hereafter referred to as "Choice contrast"); (2) parametric modulation by (relative) LL amount ("LL Amount"); and (3) parametric modulation by delay ("Delay"). Contrast images were gray matter masked to remove voxels that were unlikely to contain meaningful BOLD signal and individually *z*-scored to remove

differences in scale across images (and thereby make results transferable across studies and datasets).

Training and cross-validation. Training and cross-validation were performed on data from Study 1 only (Fig. 1*b*). Individual differences in delay discounting may result from how participants respond to intertemporal choices overall, from how they process future rewards and from how they process time delays. Thus, to capture a combination of functional processes that together determine delay discounting, we concatenated the contrast images for Choice, LL Amount, and Delay for each participant, resulting in a feature space that was triple the size of a single brain image. We then used LASSO-PCR (Tibshirani, 1996)—a machine learning-based regression algorithm—to train a classifier to predict log(k) across all voxel weights of the concatenated contrast images. LASSO-PCR first performs data reduction using principal component regression, thus identifying brain regions and networks that are highly correlated with each other. It then performs the LASSO algorithm, which shrinks regression weights toward zero, thus reducing the contribution of less important and more unstable components. LASSO-PCR has been shown to be advantageous for brain images for several reasons (Wager et al., 2011, 2013): it is adequate for predictions based on thousands of voxels, it takes into account multicollinearity between voxels and brain regions, and it yields interpretable results by allowing reconstruction of voxel weight maps based on PCR results.

To assess the predictive accuracy of the classifier in new subjects, we used 10-fold cross-validation. Thus, the training data were split up in 10 stratified combinations of training (90%) and test sets (10%), such that every subject's data were used for the training of the classifier in nine folds and held out in the remaining fold to independently assess the prediction–outcome correlation. Tenfold cross-validation was chosen a priori as a good compromise between maximizing the sample size in each training set and being within the range of recommended folds (between 5-fold and 10-fold; Scheinost et al., 2019; Poldrack et al., 2020). A priori set default regularization parameters were used for all machine-learning analysis to avoid biasing the model parameters to the data and thereby generating over-optimistic accuracy scores. Permutation tests [5000 iterations of randomly permuting the log(k) values] were used to generate null distributions and to assess the statistical significance of the prediction–outcome correlation and the mean absolute error. Out-of-sample predictions of log(k) were used for all correlational analysis (e.g., with BMI, age, blood markers).

Bootstrapping and thresholding. To identify the brain areas contributing the most reliable positive or negative weights, we performed a bootstrap analysis; 5000 samples with replacements were taken from the paired brain and outcome data, and the LASSO-PCR was repeated for each bootstrap sample. Two-tailed, uncorrected *p*-values were calculated for each voxel based on the proportion of weights above or below zero (Wager et al., 2011, 2013). False discovery rate (FDR) correction was applied to *p*-values to correct for multiple comparisons across the whole feature space (three combined brain maps).

Independent test set. Study 2 was used as an independent test set to assess the validity and generalizability of the brain pattern classifier developed based in Study 1 (i.e., the k-marker). For this purpose of testing its validity in an independent dataset (and for all future use of this brain-based model), the k-marker was trained on the data from all participants of Study 1. To assess the response of the predictive marker in Study 2, we calculated the matrix dot product between the k-marker and the concatenated contrast images (Choice screen onset, LL Amount, and Delay) from each participant. The dot product reflects the pattern similarity between the classifier and each participant's set of contrast images and, in sum with the intercepts of the classifier, provides a predicted value of log(k). Predictive accuracy of the marker was quantified by correlating the predicted value of log(k) with the actual log(k) values of each participant and by calculating the mean absolute error for each prediction.

Other statistical analyses. All statistical tests were performed in MATLAB, were two tailed, and used a significance criterion of $p = 0.05$. Statistical power calculations confirmed that the sample sizes in both studies were sufficiently powered (>80%) to detect correlations of $r > 0.3$ at a significance level of $p = 0.05$ (two-sided tests).

Data availability

Data from Study 2 is available in an online public repository (doi: 10.18112/openneuro.ds002843.v1.0.0). Deidentified data from Study 1 will be made available on publication. The resulting classifier patterns (k-marker) and codes to apply then to other datasets are available at: https://github.com/ldmk/k-marker. Code for analyses is available at https://github.com/canlab and on request to the first author.

Results

Individual differences in delay discounting

In Study 1 (Bonn University; $N = 110$), participants chose the SS option in an average of 43.7% of all trials (median, 48.1%) and had a fitted mean log(k) parameter of −5.70 [median log(k), −5.28 (corresponding to a k value of 0.0051)]. Choice behavior was characterized by substantial individual differences, with the percentage of SS choices ranging from 5.6% to 88.8%, and log(k) values ranging from −9.90 to −1.36 (Fig. 1*c*). Individual differences were very stable over a 7 week period (see Materials and Methods), with a test–retest reliability [correlation between baseline log(k) values and second session) of $r = 0.86$ [$p < 0.001$, 95% confidence interval (CI) = 0.80, 0.90; Fig. 1*c*].

On average, participants in Study 2 chose the SS option in 57.4% of trials (median, 60.0%) and had a fitted log(k) value of −4.08 [median log(k), −3.95; corresponding to a k of 0.0193). Again, individuals varied substantially in their intertemporal preferences, with the percentage of SS ranging from 0.8% to 99.2%, and log(k) ranging from −7.08 to −2.12 (Fig. 1*c*). As in Study 1, these individual differences were stable over time, with a test–retest reliability between baseline and postintervention (10 weeks later) measures of log(k) of $r = 0.74$ (Pearson correlation, $p < 0.001$; 95% CI = 0.63, 0.82; Fig. 1*c*). Thus, our data confirm both the substantial variability in delay discounting known from previous work (Kable and Glimcher, 2007; Pehlivanova et al., 2018) and the stability of these individual differences over time (Kirby, 2009; Anokhin et al., 2015; Lempert and Phelps, 2016), allowing us to investigate the neurofunctional bases of these individual differences.

Significant cross-validated prediction of delay discounting based on fMRI

Training (using LASSO-PCR) and cross-validating (10-fold) the predictive marker (termed k-marker; Fig. 2*a*) in Study 1 resulted in a cross-validated prediction–outcome correlation [i.e., correlation between predicted and actual log(k)] of $r = 0.49$ (permutation test, $p < 0.001$), a mean squared error of 2.84 (permutation test, $p < 0.001$), and a mean absolute error for predicted log(k) of 1.32 (permutation test, $p < 0.001$; Fig. 2*b*,*c*, additional results and random cross-validation folds). The explained variance of the prediction compared with a hypothetical mean model (prediction R^2) was $R^2 = 0.23$. Individual differences in head motion (mean absolute framewise displacement) were related to neither log(k) (Pearson correlation: $r = -0.05$, $p = 0.58$) nor predicted log (k) (Pearson correlation: $r = 0.01$, $p = 0.92$). Statistically controlling for age, education, head motion, and total brain volume (using partial correlations) did not substantially change the relationships between actual log(k) and predicted log(k) (partial correlation: $r = 0.54$, $p < 0.001$). Out-of-sample k-marker responses also predicted the percentage of SS choices (Pearson correlation: $r = 0.50$, $p < 0.001$) and log(k) calculated based on the method of Study 2 (Pearson correlation: $r = 0.45$, $p < 0.001$).

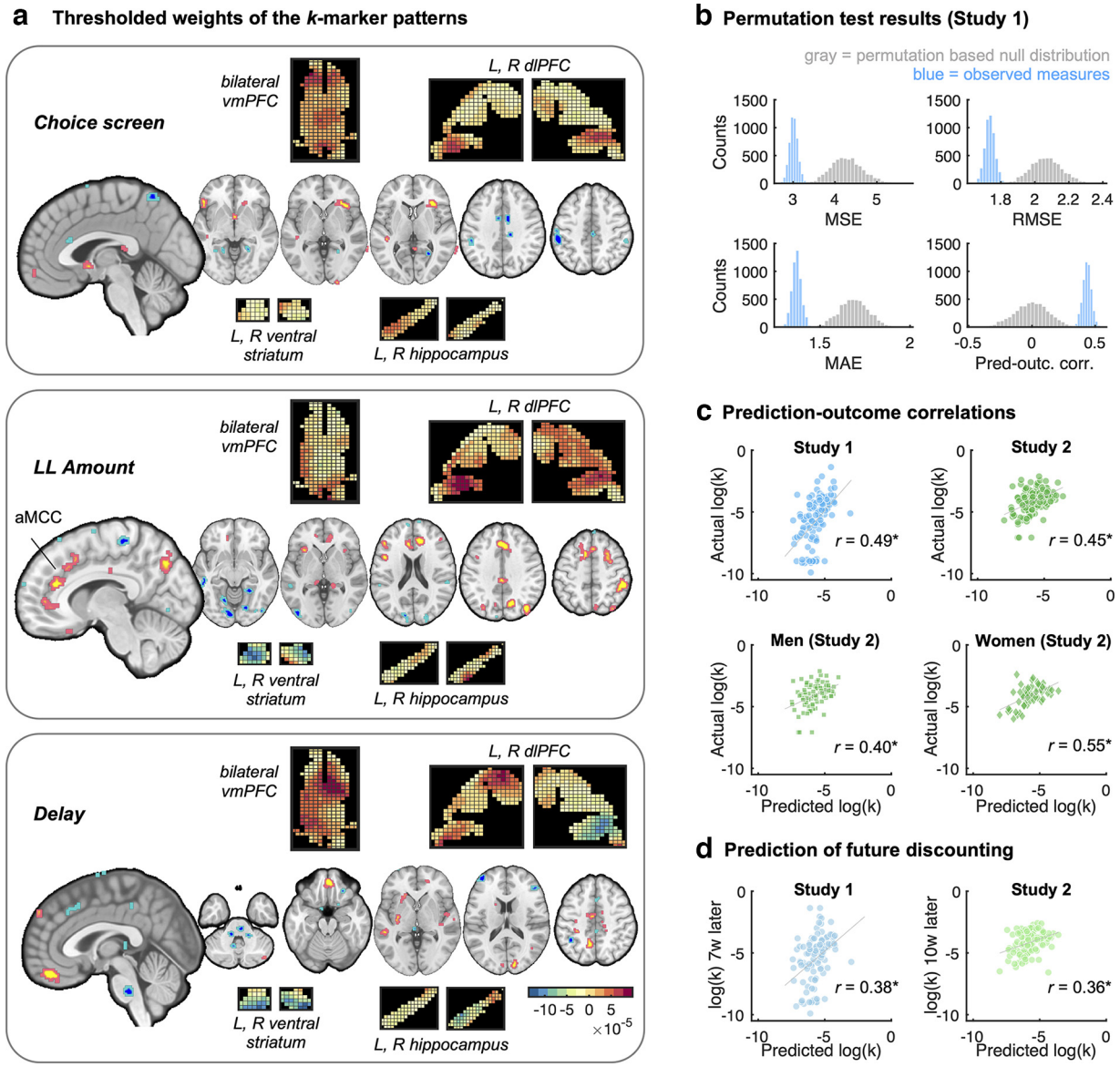

Figure 2. Weight maps and predictive accuracy of the classifier (k-marker). ***a***, Classifier weights for the three contrast images (Choice screen onset, parametric modulation by LL Amount and Delay), thresholded for illustration at $q = 0.05$ FDR corrected across the combined feature space (three concatenated maps; for coordinate tables, refer to Extended Data Figs. 2-1, 2-2, 2-3). Note that unthresholded maps are used for prediction and that the combined weights across maps are contributing to the prediction. Popout maps show the unthresholded patterns for selected regions of interest (transversal slices for vmPFC, coronal for dlPFC, and sagittal for hippocampus) to illustrate the heterogeneity of voxel weights (e.g., positive vs negative) within each region and across the three interdependent weight maps. ***b***, Results of the permutation tests (Study 1). Log(k) values were randomly permuted, and the prediction algorithm was repeated on the permuted brain–outcome data 5000 times to generate null distributions (in gray) for the following standard accuracy metrics: mean squared error (MSE), root mean squared error (RMSE), mean absolute error (mean abs error), and prediction–outcome correlation (all p-values < 0.0002). In addition, observed metrics in 5000 random cross-validation folds are shown in blue bars. ***c***, For interpretability and comparability across both studies, prediction–outcome correlations are shown as scatterplots for Study 1 ($N = 110$, $r = 0.49$, $p < 0.001$, permutation test) and Study 2 (independent validation dataset, parametric prediction–outcome correlation, $N = 145$, $r = 0.45$, $p < 0.001$, 95% CI = 0.31, 0.57). Correlations between predicted and observed log(k) values were significant in both male and female participants (Study 2). ***d***, Prediction of future discounting. Responses of the k-marker responses at baseline significantly predict individual differences in log(k) 7 weeks later in Study 1 (left panel: $N = 109$, $r = 0.38$, $p = 0.001$, 95% CI = 0.20, 0.53) and 10 weeks later in Study 2 (right panel: $N = 102$, $r = 0.36$, $p = 0.002$, 95% CI = 0.17, 0.51).

Validation of the k-marker in an independent test dataset (Study 2)

Brain markers of individual differences become more meaningful if they can be validated in different and completely independent data (Kragel et al., 2018). The validity of the marker should not depend on study-specific parameters such as the type of scanner used for data acquisition, preprocessing software, or other aspects of the data (Woo et al., 2017; Kragel et al., 2018; Scheinost et al., 2019).

We therefore tested whether the k-marker—developed and cross-validated entirely in Study 1—could predict discounting in a completely independent dataset. The validation dataset (Study 2) was acquired on a different scanner, in a different laboratory and country, and using a different participant sample and different task characteristics, and was preprocessed and analyzed using different MRI analysis software. Evaluating the performance of the k-marker in Study 2 is therefore an even stronger test than cross-validation in Study 1 alone.

For this purpose, we computed the pattern expression of the k-marker using the matrix dot product for each participant's data (contrast images for Choice, parametric modulation for LL Amount, and Delay) in Study 2. The resulting predicted log(k) values were significantly correlated with actual log(k) values (Fig. 2*c*; Pearson correlation: $r = 0.45$, $p < 0.001$; 95% CI = 0.31, 0.57; mean absolute error, 1.68) demonstrating the replicability of the k-marker in a completely independent dataset. For the transfer test to Study 2, the predicted R^2 was −3.2, indicating that, while the k-marker was very accurate in identifying the rankings among individuals, the absolute prediction values were less accurate than a hypothetical mean model.

The training and cross-validation dataset (Study 1) consisted of male participants only, which might limit the validity of the k-marker in females. We therefore assessed the accuracy of the k-marker in Study 2 separately in male and female participants (Fig. 2*c*). In male participants ($N = 88$), the prediction–outcome correlation was $r = 0.40$ (Pearson correlation, $p < 0.001$; 95% CI = 0.21, 0.56). In females ($N = 57$), the prediction–outcome correlation was $r = 0.55$ (Pearson correlation, $p < 0.001$; 95% CI = 0.34, 0.71) and thus comparable, if not superior, to the predictive accuracy in males. This demonstrates that the k-marker (despite being trained on male participants' data only) predicts delay discounting well for both male and female participants. As in Study 1, individual differences in head motion in Study 2 were related neither to log(k) (Pearson correlation: $r = 0.12$, $p = 0.14$) nor predicted log(k) (Pearson correlation: $r = 0.04$, $p = 0.59$). Statistically controlling for age, sex, education, head motion, and total brain volume did not change the relationship between predicted and actual log(k) (Partial correlation: $r = 0.44$, $p < 0.001$; 95% CI = 0.30, 0.56).

Brain-based prediction of future discounting

We next assessed whether responses of the k-marker were predictive of individual differences in delay discounting as measured several weeks later. Responses of the k-marker at baseline significantly predicted (out-of-sample) discounting behavior 7 weeks later in Study 1 (Pearson correlation: $r = 0.38$, $p < 0.001$; 95% CI = 0.20, 0.53) and 10 weeks later in Study 2 (Pearson correlation: $r = 0.36$, $p = 0.002$; 95% CI = 0.17, 0.51; Fig. 2*d*). This shows that variability in k-marker responses is driven largely by stable individual differences and their underlying neurophysiological processes.

Response of the k-marker differs between lean and overweight participants

Given previous findings of higher delay discounting in overweight and obese people (Jarmolowicz et al., 2014; Amlung et al., 2016), we next tested whether individual differences in k-marker response were associated with individual differences in body mass and overweight (as measured by BMI > 25). In contrast to previous reports (MacKillop et al., 2011; Amlung et al., 2016) that have studied this relationship more systematically, actual log(k) was not significantly correlated with BMI in either of the two samples (Pearson correlations: Study 1: $r = 0.07$, $p = 0.48$; 95% CI = −0.12, 0.25; Study 2: $r = -0.04$, $p = 0.69$; 95% CI = −0.20, 0.12). However, in Study 1, response of the k-marker significantly correlated with both BMI (Pearson correlation: $r = 0.26$, $p = 0.005$; 95% CI = 0.08, 0.43; Fig. 3*a*) and percentage of body fat (Pearson correlation: $r = 0.28$, $p = 0.004$; 95% CI = 0.09, 0.45). The k-marker response in Study 1 also differed between lean participants (BMI ≤ 25) and overweight-to-obese participants (BMI > 25; two-sample *t* test: $t_{(108)} = 2.85$, $p = 0.005$, Cohen's $d = 0.55$; 95% CI = 0.12, 0.69; Fig. 3*b*). Further, the k-marker response in Study 1 significantly predicted metabolic blood markers that are associated with some of the negative health consequences of obesity, namely fasting-state insulin levels (Pearson correlation: $r = 0.22$, $p = 0.020$; 95% CI = 0.04, 0.39), measures related to insulin—HOMA-IR (a marker of insulin resistance; Pearson correlation: $r = 0.24$, $p = 0.015$; 95% CI = 0.05, 0.41), and C-peptide levels (Pearson correlation: $r = 0.23$, $p = 0.018$; 95% CI = 0.04, 0.40)—and fasting-state leptin levels (Pearson correlation: $r = 0.34$, $p = 0.001$; 95% CI = 0.16, 0.49; Fig. 3*c*). All these associations remained significant when statistically controlling for age, education, total brain volume, and average head motion.

In Study 2, the correlation between predicted log(k) and BMI was positive but not significant (Pearson correlation: $r = 0.09$, $p = 0.28$; 95% CI = −0.07, 0.25). However, paralleling the findings in Study 1, overweight-to-obese participants had a significantly higher k-marker response (higher predicted discounting)

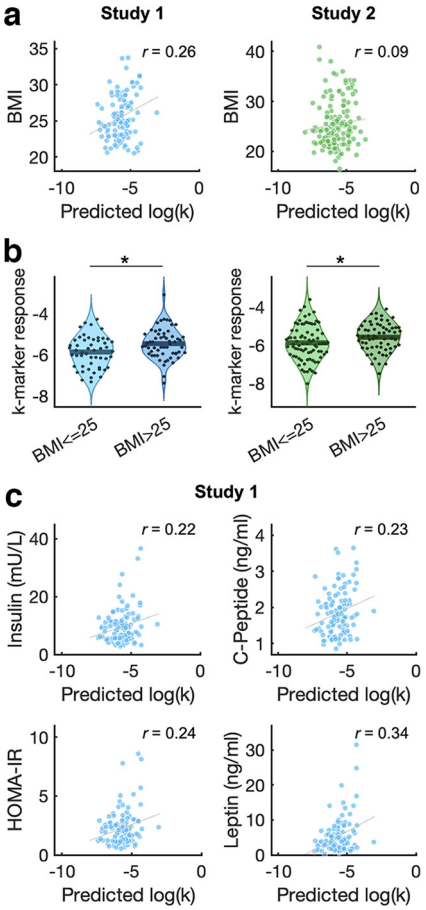

Figure 3. Association of k-marker response with BMI, overweight, and metabolic blood markers. ***a***, The k-marker response was positively and significantly correlated with BMI in Study 1 ($N = 110$, $r = 0.26$, $p = 0.005$, 95% CI = 0.08, 0.43), but not significantly in Study 2 ($N = 145$, $r = 0.09$, $p = 0.28$, 95% CI = −0.07, 0.25). ***b***, In both studies, k-marker response was significantly greater (predicting more delay discounting) in overweight participants (BMI > 25) compared with lean participants (Study 1: $t_{(108)} = 2.85$, $p = 0.005$, Cohen's $d = 0.55$, 95% CI = 0.12, 0.69; Study 2: $t_{(143)} = 2.11$, $p = 0.037$, Cohen's $d = 0.35$, 95% CI = 0.02, 0.57). Lean and overweight participants did not differ on any demographic variables in both studies (Table 1). ***c***, Individual differences in out-of-sample k-marker response in Study 1 were positively and significantly correlated with serum insulin ($N = 110$, $r = 0.22$, $p = 0.020$, 95% CI = 0.04, 0.39), C-peptide ($N = 110$, $r = 0.23$, $p = 0.018$, 95% CI = 0.04, 0.40), insulin resistance (as measured by the HOMA-IR index; $N = 105$, $r = 0.24$, $p = 0.015$, 95% CI = 0.05, 0.41), and leptin ($N = 102$, $r = 0.34$, $p = 0.001$, 95% CI = 0.16, 0.49).

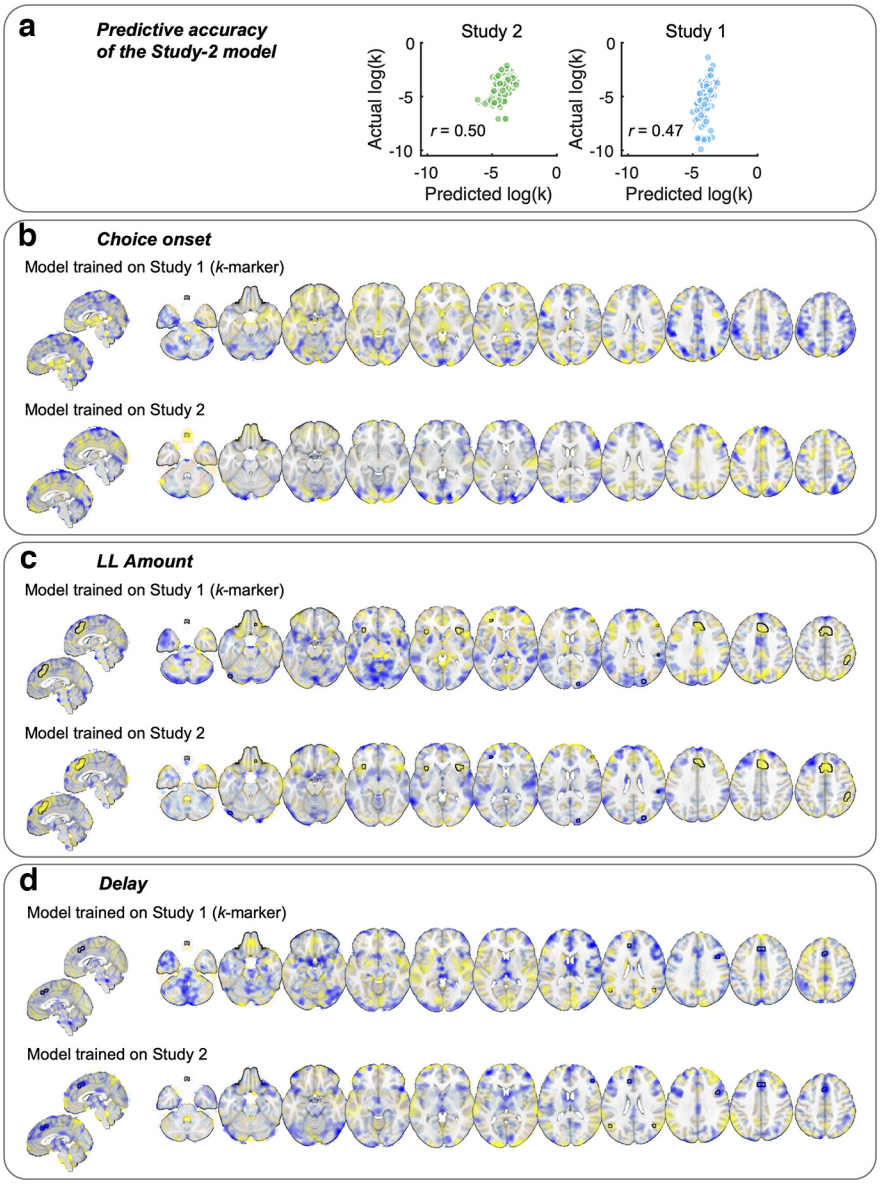

Figure 4. Results for an alternative model trained on the data from Study 2 and comparison of weight maps (control analysis). ***a***, Training and cross-validating an alternative predictive model on the data from Study 2 ($N = 145$) resulted in a prediction–outcome correlation of $r = 0.50$ (comparable to the original predictive model) and a prediction $R^2 = 0.25$. Testing this model on the data of Study 1 ($N = 110$, as an independent test set) resulted in a prediction–outcome correlation of $r = 0.47$ and a prediction $R^2 = -0.61$. ***b–d***, The contrast-wise unthresholded weight maps of the two different predictive models are displayed in ***b*** (for the Choice contrast), ***c*** (LL Amount), and ***d*** (Delay). Yellow indicates positive, and blue indicates negative voxel weights, with lower transparencies indicating stronger absolute weights. Black outlines reflect the conjunction of significant feature weights in both models (at $p < 0.05$ corrected for multiple comparisons in each model). The correlation between feature weights correlated of the two models was $r = 0.09$ (across all three maps). Correlations for the LL Amount ($r = 0.10$) and Delay contrast ($r = 0.11$) were numerically higher than for the Choice screen contrast ($r = 0.05$).

compared with lean participants (two-sample t test: $t_{(143)} = 2.11$, $p = 0.037$; Cohen's $d = 0.35$; 95% CI = 0.02, 0.57; Fig. 3*b*).

Thresholded activation patterns of the k-marker

Activation patterns across the whole-brain gray matter and across all three contrasts are used for prediction and cross-validation. To identify the areas that contributed the most strongly with positive or negative weights, we used a bootstrapping procedure (5000 samples). Bootstrapped weights were thresholded at $q = 0.05$ FDR corrected across the whole weight map of the combined feature space (Fig. 2*a*, Extended Data Figs. 2-1, 2-2, 2-3).

Our results revealed a distributed network of areas that jointly contributed to individual differences in delay discounting, including the ventromedial prefrontal cortex (vmPFC), ventral striatum, anterior midcingulate cortex (aMCC), hippocampus, and frontoparietal and visual areas (Fig. 2). Predictive activity patterns differed for the processes captured by the three different contrast images. Of note, some regions showed negative weights (i.e., predicted less discounting) for one contrast but positive weights (i.e., predicted more discounting) for another. For the Choice (vs implicit baseline) contrast, activity in the striatum, the anterior insula (AI), and lateral prefrontal areas contributed positive weights for more discounting, whereas activity in visual, premotor, and motor areas contributed negative weights. For the parametric modulation by LL Amount, activity in vmPFC, aMCC, posterior cingulate cortex, precuneus, and frontoparietal areas contributed positive weights for greater discounting, whereas visual areas and premotor areas contributed mainly negative weights. For the parametric modulation by Delay, we observed positive weights in the most ventral part of the vmPFC, premotor areas, and visual cortex, and negative weights in frontoparietal areas and brainstem regions.

To further assess the stability of weights, we tested whether developing the predictive model on the data of Study 2 and testing on Study 1 would yield comparable results. Training and cross-validating the model on the data of Study 2 resulted in similar prediction and transfer accuracy (Fig. 4) and qualitatively similar weight maps (Fig. 4). At the FDR-corrected level, voxels with significant weights in both directions (conjunction null; Nichols et al., 2005) for the LL Amount contrast were found in aMCC, bilateral AI, vmPFC, ventrolateral PFC, dorsolateral PFC (dlPFC), intraparietal sulcus, visual cortex, and cerebellum. For the Delay contrast, significant weights in both directions were found in aMCC, dlPFC, parietal cortex, and AI. No voxels survived FDR correction in both directions for the Choice contrast.

Training predictive patterns on the three contrasts separately resulted in lower predictive accuracies (Fig. 5).

Similarity of k-marker brain patterns to meta-analytic maps

We next compared the predictive maps of the k-marker with term-based meta-analytic images (Yarkoni et al., 2011) for processes that may contribute to intertemporal decision-making. We computed the spatial correlation (Pearson's r) between the k-marker and meta-analytic maps for (1) affective- and value-related, (2) conflict-related and cognitive control-related, and (3) memory-related terms (Fig. 6). While these spatial correlations

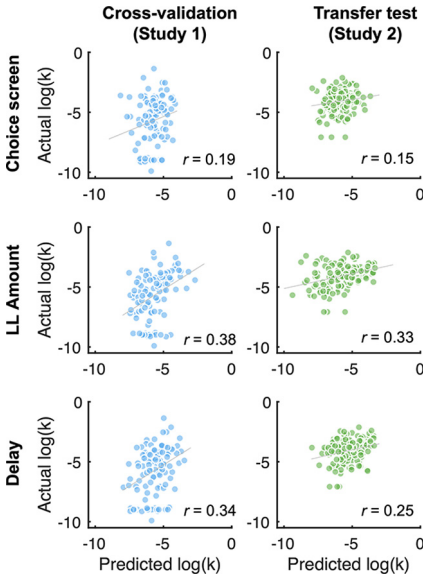

Figure 5. Results (prediction–outcome correlations) for training separate predictive models for each of the three contrasts (control analysis). To assess their distinct contributions, we trained three separate predictive models on each of the three contrast maps of Study 1 and tested them on the corresponding contrast maps of Study 2 (using the same algorithm and cross-validation procedure as before). The results showed modest predictive accuracy for the model trained on the Choice screen contrast only (top row), with a prediction–outcome correlation of $r = 0.19$ in Study 1 (training and cross-validation set, $p = 0.10$ based on permutation test, 5000 iterations) and of $r = 0.15$ in Study 2 ($p = 0.07$). Training a model based on the LL Amount contrast had a significant prediction–outcome correlation of $r = 0.38$ in Study 1 ($p < 0.001$, permutation test) and of $r = 0.34$ ($p < 0.001$) in Study 2. Similarly, training a model on the Delay contrast resulted in significant prediction–outcome correlations of $r = 0.34$ in Study 1 ($p = 0.014$, permutation test) and of $r = 0.25$ ($p = 0.002$) in Study 2. Thus, none of the separate models achieved a similarly high predictive performance as the combined model (three concatenated contrasts), especially regarding transfer to Study 2.

are descriptive (Koban et al., 2019), they can inform us quantitatively whether and in which direction (positive or negative) previously identified functional networks contribute to individual differences in delay discounting.

Value-related and affect-related maps (especially "affect" and "emotion") showed consistent positive correlations (r values > 0.05) with the Choice-related pattern of the k-marker, in line with the idea that more affect-related activity during intertemporal choices leads to more impatient decisions. However, stronger engagement of affective and especially "reward"-related and "value"-related activity for increasing LL Amount (and, to a lesser extent, for increasing delays) was associated with less discounting. This suggests that lower discounting is associated with greater sensitivity of valuation-related signals to the amount of LL rewards.

In contrast to our initial hypothesis, more activity in cognitive control-related areas was not associated with lower discounting. Instead, there were positive correlations (r value range, 0.05–0.19) of the Choice pattern with meta-analytic maps for "attention," "cognitive control," "conflict," and "executive" (i.e., more positive weights predicting greater discounting). Further, stronger activation of control-related maps by greater LL Amount was associated with greater discounting, whereas stronger activation of control-related activity for longer delays was associated with less discounting.

Finally, we assessed the contribution of brain systems related to memory and prospection. While the term "memory" (which also includes working-memory studies) showed a pattern similar to that for control-related maps, more specific terms such as "episodic memory," "imagery," and "planning" were not substantially positively or negatively correlated with any of the k-marker patterns (r values approximately ≤ 0.05).

Parallel findings were obtained when testing whether activity in nonoverlapping meta-analytic maps (Yarkoni et al., 2011; for value-related, cognitive control-related, or episodic memory-related activity) could separately predict log(k) (Fig. 7). Whereas areas associated with "cognitive control" showed significant prediction in Study 1 and transfer to Study 2, areas associated with value predicted discounting in Study 1 but no significant transfer to Study 2. Areas associated with episodic memory showed only marginal prediction in Study 1 and no significant transfer to Study 2.

Local prediction of log(k)

Finally, we assessed whether activity patterns in smaller, more local brain areas could predict out-of-sample log(k) in Study 1 and whether such predictions would accurately transfer to Study 2. For this purpose, we used an established multimodal cortical parcellation (Glasser et al., 2016) in combination with several other, subcortical parcellations (Diedrichsen et al., 2009; Shen et al., 2013; Bär et al., 2016; Pauli et al., 2016), resulting in a total of 485 regions (publicly available at https://github.com/canlab/Neuroimaging_Pattern_Masks/tree/master/Atlases_and_parcellations/2018_Wager_combined_atlas). We trained and cross-validated a separate classifier for each region (combining functional activity across all three contrasts). For each region, we then tested whether the patterns trained on Study 1 data were predictive of individual differences in Study 2. Activity patterns that consistently predicted delay discounting in both studies were found in mid-cingulate cortex and posterior cingulate cortex, right insula, and lateral frontal and parietal areas (Fig. 8, Table 2), in line with the contributions of these areas in the whole-brain predictive pattern. In addition, activity patterns in amygdala, hippocampus, basal ganglia, and brainstem areas (periaqueductal gray) also predicted individual differences in delay discounting in both studies.

Discussion

A major goal of neuroscience and psychiatry is to identify neuromarkers of transdiagnostic processes that are altered across different diseases or predispose individuals to such diseases (Insel and Cuthbert, 2015). Delay discounting—how much people prefer sooner compared with future rewards—has been proposed as such a transdiagnostic process across obesity and various forms of psychopathology, especially addiction and eating disorders (Bickel et al., 2014; Amlung et al., 2019; Lempert et al., 2019). In this article, we advanced our understanding of the brain processes that drive variability in decision-making by identifying a distributed pattern of functional brain activity that predicts individual differences in delay discounting. We first used a cross-validation procedure to develop a novel functional brain marker of delay discounting (k-marker) based on whole-brain, gray matter-masked fMRI data ($N_1 = 110$). We then validated the k-marker (trained on Study 1 data only) in an independent second fMRI dataset ($N_2 = 145$), sampled in a cohort with different sociodemographic characteristics, on a different fMRI scanner, and using a different delay discounting task. Prediction–outcome correlations were 0.49 (Study 1) and 0.45 (Study 2), as large or larger than the prediction of individual differences in other domains reported in previous studies (Rosenberg et al., 2016; Beaty et al., 2018; Han et al., 2022). In both studies, individual differences in discounting were stable over time,

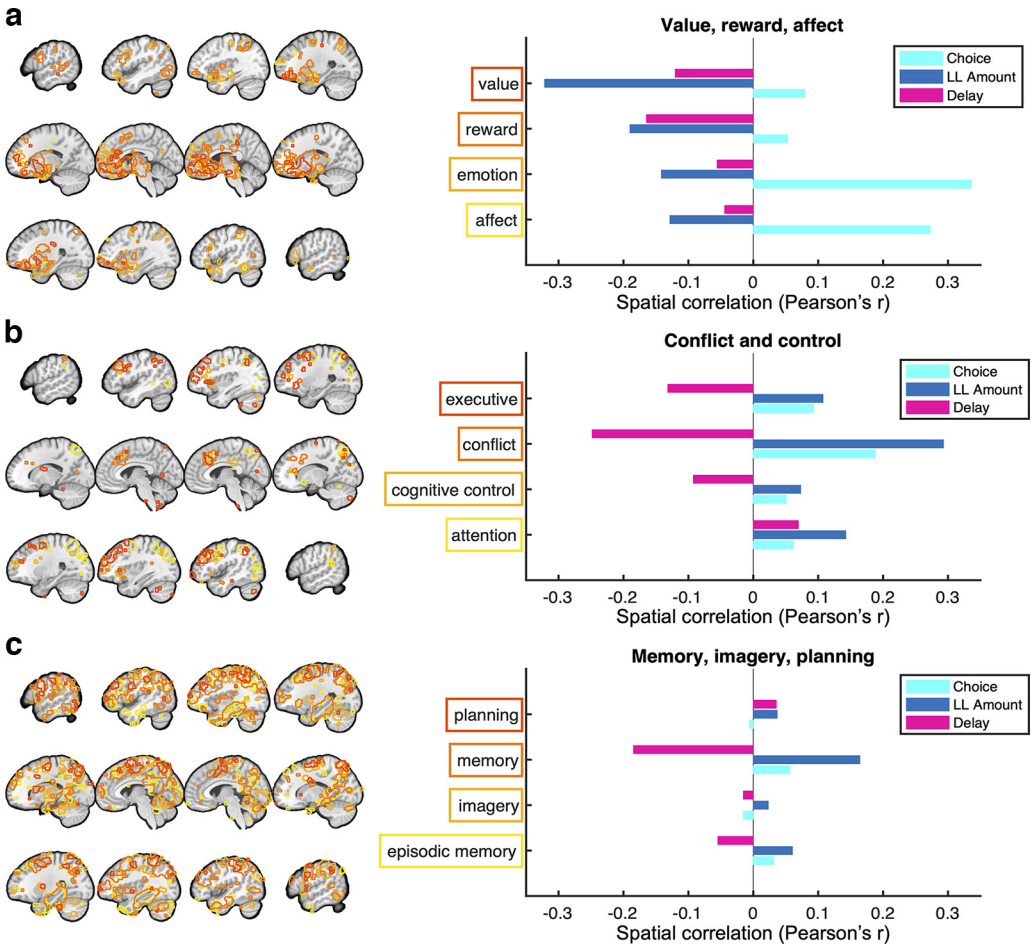

Figure 6. Spatial similarity of the k-marker with meta-analytic maps. ***a–c***, To quantitatively compare the classifier patterns with theoretically relevant functional networks, we computed the spatial correlation of the unthresholded k-marker patterns with thresholded Neurosynth meta-analytic maps (Yarkoni et al., 2011) associated with value, reward, and affect (***a***); conflict and control (***b***); and memory, imagery, and planning (***c***). Meta-analytic maps from each group of terms are overlaid on the left (outline colors matching the outlines of the terms on the right) and can be inspected in greater detail online (www.Neurosynth.org). Note that spatial correlations are purely descriptive, indicating whether activity in any of the shown functional maps is positively ($r > 0$) or negatively ($r < 0$) associated with discounting for each component map of the k-marker (Choice, LL Amount, Delay).

and k-marker responses measured at baseline significantly predicted behavior several weeks later.

Recent findings have questioned the utility of brain imaging in predicting individual differences, especially for structural and resting-state fMRI data and for univariate, voxelwise associations (Marek et al., 2022). An important advance of the present study is that it overcomes many of the limitations of previous studies by providing an independently cross-validated and multivariate "brain model" (Kragel et al., 2018) of stable individual differences in impatient decision-making, in line with recent recommendations on studying brain-based prediction of individual differences (Rosenberg and Finn, 2022). As such, this brain model can be directly tested, validated, or refined in other existing or future fMRI datasets acquired during an intertemporal choice task. Its predictive performance can also be tested in clinical populations, such as patients with severe obesity, eating or substance use disorders, and other types of psychopathology.

Our results also inform the debate regarding the contributions of specific brain regions and functional networks to individual differences in delay discounting. Among the brain areas that contributed with positive and/or negative weights were the vmPFC, striatum, and other regions associated with valuation and reward (Levy and Glimcher, 2011; Bartra et al., 2013; Clithero and Rangel, 2014). This finding is in line with previous, univariate findings (Cooper et al., 2013; Pehlivanova et al., 2018; MacNiven et al., 2020). The present results add to this emergent picture by showing that greater sensitivity of reward-related and value-related areas to the amount of the LL reward is linked to more patient decision-making.

Significant weights were found most consistently in the frontoparietal areas, midcingulate cortex, and anterior insula. Activity in these areas also allowed for significant prediction based on local activity alone [Fig. 8, region of interest (ROI) analysis]. The dlPFC has been theorized to implement self-control and far-sighted decision-making (McClure et al., 2004; Hare et al., 2014). Yet the present results are surprising as they draw a more complex picture of the contributions of these areas to delay discounting, with modulation of these areas by greater LL rewards being positively associated with discounting and modulation by delay being negatively associated with discounting. Thus, areas meta-analytically associated with cognitive control were recruited more for long delays and small LL amounts for low discounters, and for shorter delays and larger LL amounts for high discounters. These are the cases in which decisions are most difficult (closer to the indifference point) and therefore require resolution of response conflict (Botvinick et al., 2001; Kool et al., 2013; Shenhav et al., 2013; Hutcherson et al., 2020) or integration of expected value and risk of future rewards (Tobler et al., 2009).

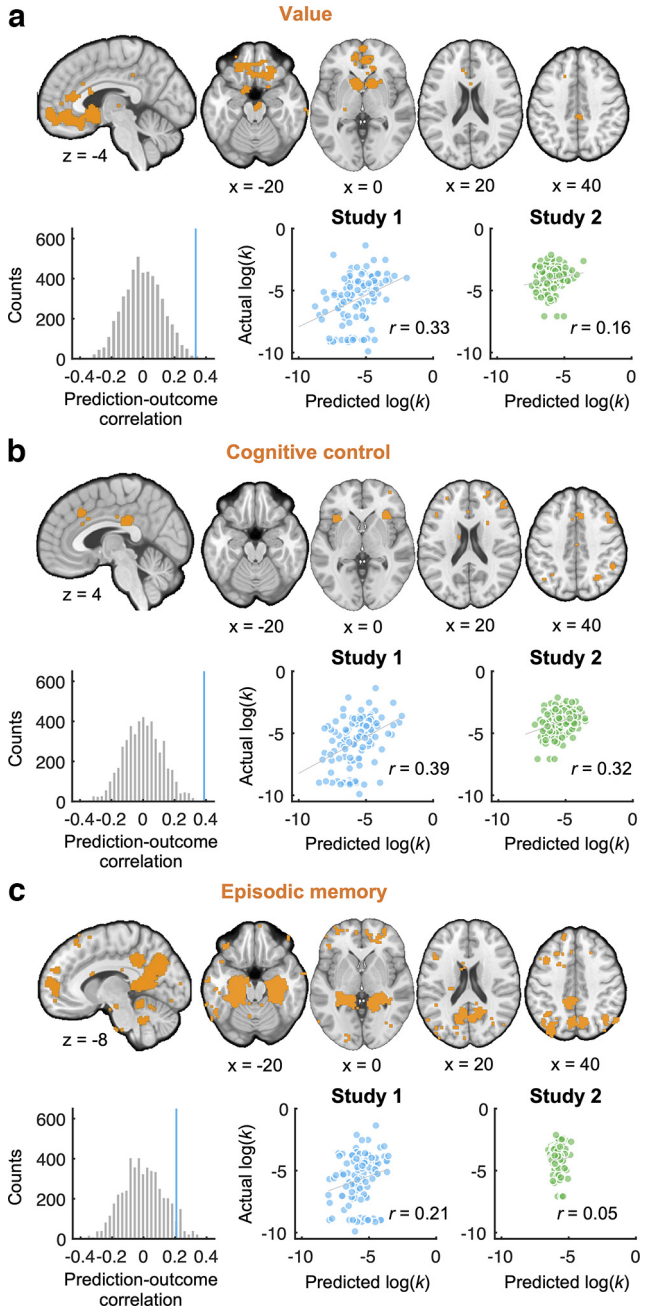

Figure 7. Results for training separate predictive models in three different meta-analytic maps. ***a–c***, Term-based meta-analytic maps for value (***a***), cognitive control (***b***), and episodic memory (***c***) were downloaded from Neurosynth (Yarkoni et al., 2011). To obtain nonoverlapping maps (displayed in orange), we masked by excluding voxels that were part of any of the other two maps. We then trained and cross-validated predictive patterns of individual differences in log(k) in the data of Study 1 (blue scatter plots) and further tested the performance of these patterns in Study 2 (green scatter plots). While activity in cognitive control-related areas led to significant cross-validated prediction in Study 1 and significant transfer to Study 2, such effects were weaker for value or episodic memory-related areas.

These findings have implications for models of delay discounting and self-control in cognitive neuroscience. First, they speak against the idea of a simple dual process account of intertemporal choice and self-control (McClure et al., 2004), joining previous work that has suggested more complex neural processes at play (Kable and Glimcher, 2007; Ballard and Knutson, 2009; Hare et al., 2014; Berkman et al., 2017). Second, they also speak against the idea that more frontoparietal activity is related to higher individual levels of self-control. Instead, they suggest that for which choice options control-related areas are activated is more informative than their overall level of activation. This finding is in line with value-based choice models of self-control (Berkman et al., 2017) and with recent evidence that high and low discounters differ in how much attention they allocate to amount versus delay information (Amasino et al., 2019). It also fits with the idea that low discounters may not need "control" to discount less (Lempert et al., 2019), and that high discounters may use cognitive control for different types of decisions.

In line with the importance of prospection and self-projection in intertemporal decision-making, the hippocampus and adjacent midtemporal areas have been associated with individual differences in discounting (Benoit et al., 2011; Peters and Büchel, 2011; Lebreton et al., 2013). The k-marker has significant weights in parahippocampal areas and in occipital areas, but the weight maps were not strongly associated with broader meta-analysis-based activation maps of episodic memory or prospection, possibly because those masks also include many areas that are involved in processes other than memory and prospection. In agreement with the k-marker results and the literature described above, our ROI-based results showed significant local prediction of individual differences in delay discounting in hippocampus, amygdala, and the memory-related anteromedial thalamus.

Our findings highlight the importance of investigating distributed brain activity patterns, confirming the notion that delay discounting depends on the interactions among different functional processes and networks in the brain. In addition to frontoparietal areas, midcingulate, and hippocampus, several other cortical and subcortical areas also allowed for cross-validated local prediction of individual differences in delay discounting, across both datasets. Consistent with the whole-brain results, these included several areas in the mid-insula and posterior insula, which are involved in interoception (Craig, 2009), salience (Bartra et al., 2013), and exploration (Zhen et al., 2022)—processes that may all be involved in delay discounting. Local prediction was also found in subcortical areas associated with affect and visceromotor control, including the amygdala and the periaqueductal gray.

Previous work has related individual differences in delay discounting with obesity, substance use disorders, and psychiatric diseases (Peters and Büchel, 2011; Amlung et al., 2019; Lempert et al., 2019). In the two samples presented here, log(k) values based on participants' choices themselves were not significantly associated with BMI or overweight. However, the two studies were not designed to include a large range of BMI or many obese participants, and obesity-related alterations in discounting might be more pronounced for food than monetary rewards. While in Study 1 participants' height and weight were measured by the experimenters, these values were self-reported in Study 2, which might explain the lower associations with BMI in Study 2.

In contrast to discounting behavior, responses to the k-marker significantly differed between lean and overweight participants and predicted out-of-sample blood markers related to glucose and fat metabolism. These findings suggest that this functional brain marker reflects variance in neurophysiology that is related to stable long-term patterns in decision-making and health. The k-marker even seemed more sensitive to individual differences than the behavioral measures it was trained on, potentially because it is a closer reflection of the neurophysiological underpinnings that drive both discounting behavior and more distal health outcomes, in line with previous evidence that brain-based prediction can

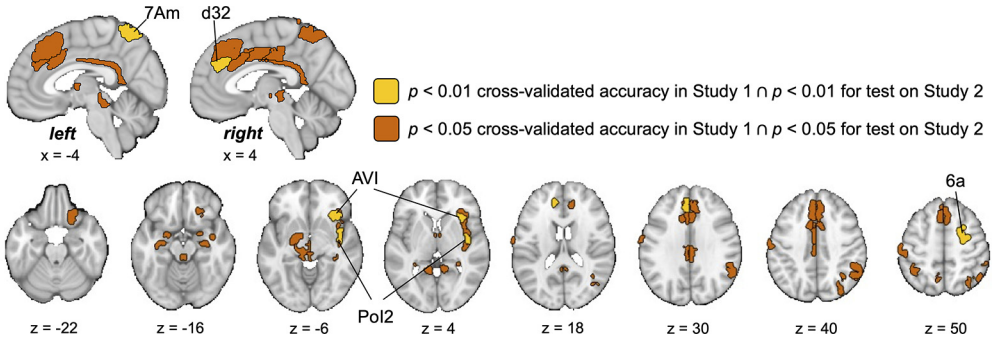

Figure 8. ROI-based prediction of individual differences in discounting. An established cortical parcellation (Glasser et al., 2016) together with a combination of subcortical parcellations (see atlas available on Github: https://github.com/canlab/Neuroimaging_Pattern_Masks/tree/master/Atlases_and_parcellations/2018_Wager_combined_atlas) was used to test whether functional activity across all three contrasts (Choice, LL Amount, and Delay) in local brain areas could predict individual log(k) values. ROIs that resulted in significant cross-validated prediction in Study 1 and significant transfer to Study 2 are shown in yellow ($p = 0.01$ uncorrected for multiple comparisons in both studies) and orange ($p = 0.05$ uncorrected in both studies). They included areas in the mid-cingulate and posterior cingulate, dorsomedial prefrontal cortex, several regions in the right insula, lateral frontoparietal regions, hippocampus, amygdala, thalamus, and brainstem areas.

Table 2. ROI-based prediction of individual differences in log(k)

			Study 1 (training and cross-validation)		Study 2 (test)	
Area name	Area description	Hemisphere	Prediction–outcome (*r*)	*p*-value	Prediction–outcome (*r*)	*p*-value
RSC	RetroSplenial complex	L	0.30	0.010	0.21	0.010
RSC	RetroSplenial complex	R	0.23	0.049	0.21	0.013
23d	Area dorsal 23	L	0.23	0.042	0.17	0.043
7Am	Medial area 7a	L	0.23	0.045	0.22	0.007
7Am	Medial area 7a	R	0.30	0.009	0.28	0.001
7PC	Area 7PC	R	0.28	0.016	0.20	0.014
Area1	Area 1	L	0.23	0.037	0.18	0.035
p24pr	Area posterior 24 prime	L	0.30	0.014	0.21	0.011
a24pr	Area anterior 24 prime	L	0.38	0.001	0.21	0.013
a24pr	Area anterior 24 prime	R	0.37	0.001	0.21	0.010
p32pr	Area posterior 32 prime	L	0.43	0.000	0.20	0.016
d32	Area dorsal 32	L	0.36	0.002	0.24	0.004
d32	Area dorsal 32	R	0.28	0.016	0.34	0.000
8BM	Area 8BM	L	0.25	0.033	0.29	0.000
8BM	Area 8BM	R	0.30	0.012	0.26	0.001
13l	Area 13l	R	0.25	0.025	-0.16	0.048
6a	Area 6 anterior	R	0.40	0.001	0.30	0.000
Pol2	Posterior insular area 2	R	0.35	0.004	0.21	0.009
MI	Middle insular area	R	0.23	0.040	0.39	0.000
AVI	Anterior ventral insular area	R	0.30	0.009	0.43	0.000
TPOJ3	Temporo-parieto-occipital Junction 3	R	0.28	0.017	0.20	0.018
IP1	Area intraparietal11	R	0.29	0.013	0.23	0.006
PFm	Area PFm complex	R	0.25	0.028	0.24	0.003
Pol1	Posterior insular area 1	R	0.24	0.041	0.27	0.001
FOP5	Area frontal opercular 5	R	0.27	0.022	0.36	0.000
GPi	Internal globus pallidus	R	0.23	0.046	0.23	0.005
Thal_AM	Anteromedial thalamic nucleus	L	0.27	0.024	0.19	0.020
Bstem Midbd	Brainstem midbrain	L	0.23	0.047	0.22	0.008
Bstem PAG	Brainstem periaqueductal gray	R&L	0.39	0.001	0.19	0.023
CA2 Hippocampus	Hippocampus area CA2	R&L	0.22	0.040	0.20	0.015
Amygdala CM	Centromedial amygdala	R&L	0.22	0.038	0.17	0.042

L, Left; R, right. This analysis used an existing atlas of the brain, including 485 regions based on several different previous parcellations (Diedrichsen et al., 2009; Shen et al., 2013; Bär et al., 2016; Glasser et al., 2016; Pauli et al., 2016; available at: https://github.com/canlab/Neuroimaging_Pattern_Masks/tree/master/Atlases_and_parcellations/2018_Wager_combined_atlas). Predictive patterns were trained and cross-validated using Study 1 data only (using the same procedures as for the global classifier) and then tested in Study 2. The table below shows only brain parcels that had significant prediction in both datasets (*p*-values are uncorrected for multiple comparisons). Note that each parcel contains many voxels, each of which may contribute with positive and/or negative weights to delay discounting for each of the three contrast images.

outperform behavior-based prediction (Genevsky et al., 2017). Of note, our approach is cross-sectional and remains agnostic regarding potential causal links among brain function, behavior, and body weight. While higher discounting is typically considered a causal or predisposing factor for weight gain, an alternative hypothesis is that overweight and changes in metabolism lead to changes in brain physiology and subsequent behavioral outcomes (Schmidt et al., 2021; Cornil et al., 2022). Future work can test the k-marker in larger numbers of participants with obesity and other health conditions.

In conclusion, the k-marker—a novel fMRI-based brain signature—predicts individual differences in intertemporal decision-making in neurotypical, healthy adults across different populations, scanners, and analysis pipelines. It can be

quantitatively tested in any other fMRI study on delay discounting for which contrast images for Choice, LL Amount, and Delay can be computed, including in other delay-discounting paradigms, such as those that involve nonmonetary rewards such as food or social discounting tasks (Jones and Rachlin, 2006; Strombach et al., 2015). Future work could test the generalizability of the k-marker in children, adolescents, the elderly, or clinical populations. Most importantly, future work will show whether the k-marker prospectively predicts clinical status and health outcomes in conditions related to abnormal discounting, such as eating disorders, substance use, and other psychiatric disorders.

References

Amasino DR, Sullivan NJ, Kranton RE, Huettel SA (2019) Amount and time exert independent influences on intertemporal choice. Nat Hum Behav 3:383–392.

Amlung M, Petker T, Jackson J, Balodis I, MacKillop J (2016) Steep discounting of delayed monetary and food rewards in obesity: a meta-analysis. Psychol Med 46:2423–2434.

Amlung M, Marsden E, Holshausen K, Morris V, Patel H, Vedelago L, Naish KR, Reed DD, McCabe RE (2019) Delay discounting as a transdiagnostic process in psychiatric disorders: a meta-analysis. JAMA Psychiatry 76:1176–1186.

Anokhin AP, Golosheykin S, Mulligan RC (2015) Long-term test-retest reliability of delayed reward discounting in adolescents. Behav Processes 111:55–59.

Audrain-McGovern J, Rodriguez D, Epstein LH, Cuevas J, Rodgers K, Wileyto EP (2009) Does delay discounting play an etiological role in smoking or is it a consequence of smoking? Drug Alcohol Depend 103:99–106.

Ballard K, Knutson B (2009) Dissociable neural representations of future reward magnitude and delay during temporal discounting. Neuroimage 45:143–150.

Bär K-J, de la Cruz F, Schumann A, Koehler S, Sauer H, Critchley H, Wagner G (2016) Functional connectivity and network analysis of midbrain and brainstem nuclei. Neuroimage 134:53–63.

Bartra O, McGuire JT, Kable JW (2013) The valuation system: a coordinate-based meta-analysis of BOLD fMRI experiments examining neural correlates of subjective value. Neuroimage 76:412–427.

Beaty RE, Kenett YN, Christensen AP, Rosenberg MD, Benedek M, Chen Q, Fink A, Qiu J, Kwapil TR, Kane MJ, Silvia PJ (2018) Robust prediction of individual creative ability from brain functional connectivity. Proc Natl Acad Sci U S A 115:1087–1092.

Benoit RG, Gilbert SJ, Burgess PW (2011) A neural mechanism mediating the impact of episodic prospection on farsighted decisions. J Neurosci 31:6771–6779.

Berkman ET, Hutcherson CA, Livingston JL, Kahn LE, Inzlicht M (2017) Self-control as value-based choice. Curr Dir Psychol Sci 26:422–428.

Berman MG, Yourganov G, Askren MK, Ayduk O, Casey BJ, Gotlib IH, Kross E, McIntosh AR, Strother S, Wilson NL, Zayas V, Mischel W, Shoda Y, Jonides J (2013) Dimensionality of brain networks linked to life-long individual differences in self-control. Nat Commun 4:1373.

Bickel WK, Odum AL, Madden GJ (1999) Impulsivity and cigarette smoking: delay discounting in current, never, and ex-smokers. Psychopharmacology (Berl) 146:447–454.

Bickel WK, George Wilson A, Franck CT, Terry Mueller E, Jarmolowicz DP, Koffarnus MN, Fede SJ (2014) Using crowdsourcing to compare temporal, social temporal, and probability discounting among obese and non-obese individuals. Appetite 75:82–89.

Botvinick MM, Braver TS, Barch DM, Carter CS, Cohen JD (2001) Conflict monitoring and cognitive control. Psychol Rev 108:624–652.

Clithero JA, Rangel A (2014) Informatic parcellation of the network involved in the computation of subjective value. Soc Cogn Affect Neurosci 9:1289–1302.

Cooper N, Kable JW, Kim BK, Zauberman G (2013) Brain activity in valuation regions while thinking about the future predicts individual discount rates. J Neurosci 33:13150–13156.

Cornil Y, Plassmann H, Aron-Wisnewsky J, Poitou-Bernert C, Clément K, Chabert M, Chandon P (2022) Obesity and responsiveness to food marketing before and after bariatric surgery. J Consum Psychol 32:57–68.

Craig ADB (2009) How do you feel–now? The anterior insula and human awareness. Nat Rev Neurosci 10:59–70.

Diedrichsen J, Balsters JH, Flavell J, Cussans E, Ramnani N (2009) A probabilistic MR atlas of the human cerebellum. Neuroimage 46:39–46.

Fernie G, Peeters M, Gullo MJ, Christiansen P, Cole JC, Sumnall H, Field M (2013) Multiple behavioural impulsivity tasks predict prospective alcohol involvement in adolescents. Addiction 108:1916–1923.

Gabrieli JDE, Ghosh SS, Whitfield-Gabrieli S (2015) Prediction as a humanitarian and pragmatic contribution from human cognitive neuroscience. Neuron 85:11–26.

Genevsky A, Yoon C, Knutson B (2017) When brain beats behavior: neuroforecasting crowdfunding outcomes. J Neurosci 37:8625–8634.

Glasser MF, Coalson TS, Robinson EC, Hacker CD, Harwell J, Yacoub E, Ugurbil K, Andersson J, Beckmann CF, Jenkinson M, Smith SM, Van Essen DC (2016) A multi-modal parcellation of human cerebral cortex. Nature 536:171–178.

Han X, Ashar YK, Kragel P, Petre B, Schelkun V, Atlas LY, Chang LJ, Jepma M, Koban L, Losin EAR, Roy M, Woo C-W, Wager TD (2022) Effect sizes and test-retest reliability of the fmri-based neurologic pain signature. Neuroimage 247:118844.

Hare TA, Hakimi S, Rangel A (2014) Activity in dlPFC and its effective connectivity to vmPFC are associated with temporal discounting. Front Neurosci 8:50.

Hutcherson CA, Rangel A, Tusche A (2020) Evidence accumulation, not" self-control," explains why the dlPFC activates during normative choice. Elife 11:e65661.

Insel TR, Cuthbert BN (2015) Medicine. Brain disorders? Precisely. Science 348:499–500.

Jarmolowicz DP, Cherry JBC, Reed DD, Bruce JM, Crespi JM, Lusk JL, Bruce AS (2014) Robust relation between temporal discounting rates and body mass. Appetite 78:63–67.

Jones B, Rachlin H (2006) Social discounting. Psychol Sci 17:283–286.

Kable JW, Glimcher PW (2007) The neural correlates of subjective value during intertemporal choice. Nat Neurosci 10:1625–1633.

Kable JW, Caulfield MK, Falcone M, McConnell M, Bernardo L, Parthasarathi T, Cooper N, Ashare R, Audrain-McGovern J, Hornik R, Diefenbach P, Lee FJ, Lerman C (2017) No effect of commercial cognitive training on brain activity, choice behavior, or cognitive performance. J Neurosci 37:7390–7402.

Kirby KN (2009) One-year temporal stability of delay-discount rates. Psychon Bull Rev 16:457–462.

Kirby KN, Herrnstein RJ (1995) Preference reversals due to myopic discounting of delayed reward. Psychol Sci 6:83–89.

Koban L, Jepma M, López-Solà M, Wager TD (2019) Different brain networks mediate the effects of social and conditioned expectations on pain. Nat Commun 10:4096.

Kool W, McGuire JT, Wang GJ, Botvinick MM (2013) Neural and behavioral evidence for an intrinsic cost of self-control. PLoS One 8:e72626.

Kragel PA, Koban L, Barrett LF, Wager TD (2018) Representation, pattern information, and brain signatures: from neurons to neuroimaging. Neuron 99:257–273.

Lebreton M, Bertoux M, Boutet C, Lehericy S, Dubois B, Fossati P, Pessiglione M (2013) A critical role for the hippocampus in the valuation of imagined outcomes. PLoS Biol 11:e1001684.

Lempert KM, Phelps EA (2016) The malleability of intertemporal choice. Trends Cogn Sci 20:64–74.

Lempert KM, Steinglass JE, Pinto A, Kable JW, Simpson HB (2019) Can delay discounting deliver on the promise of RDoC? Psychol Med 49:190–199.

Levy DJ, Glimcher PW (2011) Comparing apples and oranges: using reward-specific and reward-general subjective value representation in the brain. J Neurosci 31:14693–14707.

Li N, Ma N, Liu Y, He X-S, Sun D-L, Fu X-M, Zhang X, Han S, Zhang D-R (2013) Resting-state functional connectivity predicts impulsivity in economic decision-making. J Neurosci 33:4886–4895.

Lozano R, et al. (2012) Global and regional mortality from 235 causes of death for 20 age groups in 1990 and 2010: a systematic analysis for the Global Burden of Disease Study 2010. Lancet 380:2095–2128.

MacKillop J, Amlung MT, Few LR, Ray LA, Sweet LH, Munafò MR (2011) Delayed reward discounting and addictive behavior: a meta-analysis. Psychopharmacology (Berl) 216:305–321.

MacNiven KH, Leong JK, Knutson B (2020) Medial forebrain bundle structure is linked to human impulsivity. Sci Adv 6:eaba4788.

Marek S, et al. (2022) Reproducible brain-wide association studies require thousands of individuals. Nature 603:654–660.

McClure SM, Laibson DI, Loewenstein G, Cohen JD (2004) Separate neural systems value immediate and delayed monetary rewards. Science 306:503–507.

Mole TB, Irvine MA, Worbe Y, Collins P, Mitchell SP, Bolton S, Harrison NA, Robbins TW, Voon V (2015) Impulsivity in disorders of food and drug misuse. Psychol Med 45:771–782.

Nichols T, Brett M, Andersson J, Wager T, Poline J-B (2005) Valid conjunction inference with the minimum statistic. Neuroimage 25:653–660.

Pauli WM, O'Reilly RC, Yarkoni T, Wager TD (2016) Regional specialization within the human striatum for diverse psychological functions. Proc Natl Acad Sci U S A 113:1907–1912.

Pehlivanova M, Wolf DH, Sotiras A, Kaczkurkin AN, Moore TM, Ciric R, Cook PA, Garcia de La Garza A, Rosen AFG, Ruparel K, Sharma A, Shinohara RT, Roalf DR, Gur RC, Davatzikos C, Gur RE, Kable JW, Satterthwaite TD (2018) Diminished cortical thickness is associated with impulsive choice in adolescence. J Neurosci 38:2471–2481.

Peters J, Büchel C (2011) The neural mechanisms of inter-temporal decision-making: understanding variability. Trends Cogn Sci 15:227–239.

Poldrack RA, Baker CI, Durnez J, Gorgolewski KJ, Matthews PM, Munafò MR, Nichols TE, Poline J-B, Vul E, Yarkoni T (2017) Scanning the horizon: towards transparent and reproducible neuroimaging research. Nat Rev Neurosci 18:115–126.

Poldrack RA, Huckins G, Varoquaux G (2020) Establishment of best practices for evidence for prediction: a review. JAMA Psychiatry 77:534–540.

Rosenberg MD, Finn ES (2022) How to establish robust brain–behavior relationships without thousands of individuals. Nat Neurosci 25:835–837.

Rosenberg MD, Finn ES, Scheinost D, Papademetris X, Shen X, Constable RT, Chun MM (2016) A neuromarker of sustained attention from whole-brain functional connectivity. Nat Neurosci 19:165–171.

Rosenberg MD, Casey BJ, Holmes AJ (2018) Prediction complements explanation in understanding the developing brain. Nat Commun 9:589.

Rosenberg MD, Martinez SA, Rapuano KM, Conley MI, Cohen AO, Cornejo MD, Hagler DJ Jr, Meredith WJ, Anderson KM, Wager TD, Feczko E, Earl E, Fair DA, Barch DM, Watts R, Casey BJ (2020) Behavioral and neural signatures of working memory in childhood. J Neurosci 40:5090–5104.

Scheinost D, Noble S, Horien C, Greene AS, Lake EM, Salehi M, Gao S, Shen X, O'Connor D, Barron DS, Yip SW, Rosenberg MD, Constable RT (2019) Ten simple rules for predictive modeling of individual differences in neuroimaging. Neuroimage 193:35–45.

Schmidt L, Medawar E, Aron-Wisnewsky J, Genser L, Poitou C, Clément K, Plassmann H (2021) Resting-state connectivity within the brain's reward system predicts weight loss and correlates with leptin. Brain Commun 3: fcab005.

Shen X, Tokoglu F, Papademetris X, Constable RT (2013) Groupwise whole-brain parcellation from resting-state fMRI data for network node identification. Neuroimage 82:403–415.

Shenhav A, Botvinick MM, Cohen JD (2013) The expected value of control: an integrative theory of anterior cingulate cortex function. Neuron 79:217–240.

Strombach T, Weber B, Hangebrauk Z, Kenning P, Karipidis II, Tobler PN, Kalenscher T (2015) Social discounting involves modulation of neural value signals by temporoparietal junction. Proc Natl Acad Sci U S A 112:1619–1624.

Tibshirani R (1996) Regression shrinkage and selection via the lasso. J R Stat Soc Series B Stat Methodol 58:267–288.

Tobler PN, Christopoulos GI, O'Doherty JP, Dolan RJ, Schultz W (2009) Risk-dependent reward value signal in human prefrontal cortex. Proc Natl Acad Sci U S A 106:7185–7190.

van den Bos W, Rodriguez CA, Schweitzer JB, McClure SM (2014) Connectivity strength of dissociable striatal tracts predict individual differences in temporal discounting. J Neurosci 34:10298–10310.

Wager TD, Atlas LY, Leotti LA, Rilling JK (2011) Predicting individual differences in placebo analgesia: contributions of brain activity during anticipation and pain experience. J Neurosci 31:439–452.

Wager TD, Atlas LY, Lindquist MA, Roy M, Woo C-W, Kross E (2013) An fMRI-based neurologic signature of physical pain. N Engl J Med 368:1388–1397.

Woo C-W, Chang LJ, Lindquist MA, Wager TD (2017) Building better biomarkers: brain models in translational neuroimaging. Nat Neurosci 20:365–377.

Yarkoni T, Poldrack RA, Nichols TE, Van Essen DC, Wager TD (2011) Large-scale automated synthesis of human functional neuroimaging data. Nat Methods 8:665–670.

Yu H, Koban L, Chang LJ, Wagner U, Krishnan A, Vuilleumier P, Zhou X, Wager TD (2020) A generalizable multivariate brain pattern for interpersonal guilt. Cereb Cortex 30:3558–3572.

Zhen S, Yaple ZA, Eickhoff SB, Yu R (2022) To learn or to gain: neural signatures of exploration in human decision-making. Brain Struct Funct 227:63–76.